Electron-impact ionization of Mg-like ions: S^{4+}, Cl^{5+}, and Ar^{6+}

A. M. Howald,* D. C. Gregory, F. W. Meyer, and R. A. Phaneuf
Oak Ridge National Laboratory, Oak Ridge, Tennessee 37831

A. Müller,† N. Djuric,‡ and G. H. Dunn
Joint Institute for Laboratory Astrophysics, University of Colorado and National Bureau of Standards, Boulder, Colorado 80309-0440

(Received 2 December 1985)

Absolute electron-impact ionization cross sections were measured as a function of collision energy for ions in the Mg-isoelectronic sequence S^{4+}, Cl^{5+}, and Ar^{6+}. The measurements cover the energy range from threshold to 1500 eV and show onsets due to the indirect ionization process of inner-shell excitation followed by autoionization. The relative magnitude of the indirect ionization process increases dramatically in comparison with the direct process along the sequence, a feature which is also emphasized by earlier data for Al^{+}.

I. INTRODUCTION

Electron-impact ionization of ions plays an important role in naturally occurring and man-made plasmas. There are a number of electron-ion collision processes which can lead to ionization, and systematic experimental studies along isonuclear (same element) or isoelectronic (same number of electrons) sequences may often identify trends that will contribute to a better understanding of these different processes. Systematic studies test the predictive power of theoretical methods and provide reliable information for applications of ionization cross sections and rate coefficients, such as the modeling of high-temperature plasmas[1] or the development of x-ray lasers.[2]

There are at least two electron-impact ionization processes which may be important in the present experimental study of ions in the Mg-isoelectronic sequence. The first is the direct ejection of an outer-shell electron,

$$e^- + X^{+q}(2p^6 3s^2) \rightarrow X^{+(q+1)}(2p^6 3s) + 2e^- , \quad (1)$$

and the second is excitation-autoionization (EA), the excitation of an inner-shell electron followed by autoionization; for example,

$$e^- + X^{+q}(2p^6 3s^2) \rightarrow X^{+q}(2p^5 3s^2 nl) + e^- \rightarrow X^{+(q+1)}(2p^6 3s) + 2e^- . \quad (2)$$

The cross sections for the direct-ionization process [Eq. (1)] are often approximated using the semiempirical formulas of Lotz.[3] More detailed calculations of direct ionization have been made for a number of ions in the scaled plane-wave Born (SPWB),[4] Coulomb-Born with exchange (CBE),[5] and distorted-wave with exchange (DWE) (Ref. 6) approximations.

Excitation-autoionization is sometimes included in semiempirical estimates of cross sections by using the modified Lotz formula of Burgess and Chidichimo.[7] Cross sections for EA have been calculated with mixed success for a number of ions in the CBE (Refs. 8 and 9) and DWE (Refs. 10 and 11) approximations. Calculations of cross sections for EA due to $2p$-nl excitations have been published by Griffin *et al.*,[11] Henry and Msezane,[12] and by Sampson[9] for a number of ions in the Na-isoelectronic sequence. McGuire[13] has made SPWB calculations for $2p$-nl excitations of Mg-like Al^{+}, Cl^{5+}, and Ar^{6+}, and these results are useful for estimating the EA contributions to the ionization of these ions. Accompanying the present paper are new distorted-wave calculations by Pindzola *et al.*[14] for the specific ions investigated here. Tayal and Henry[15] have made close-coupling calculations for $2p$-nl excitation of these Mg-like ions.

II. EXPERIMENTAL TECHNIQUE

These measurements were performed using crossed beams of ions and electrons.[16] The ions were produced in the new Oak Ridge National Laboratory electron cyclotron resonance (ECR) ion source.[17] Ions were extracted from the source plasma, accelerated to $10\times q$ keV, focused, and mass-analyzed by a 90° bending magnet. After being refocused and collimated, the beams entered a collision chamber in which the vacuum was maintained at approximately 2×10^{-9} Torr to reduce background counts in the ionization channel due to stripping of ions on residual gas. A schematic diagram of the chamber is shown in Fig. 1.

Typical beam currents in the collision chamber were 10 nA for $^{34}S^{4+}$ (200 nA for $^{32}S^{4+}$), 100 nA for Cl^{5+}, and 300 nA for Ar^{6+}. In the collision chamber, the multicharged ion beams were deflected through 90° by an electrostatic parallel-plate analyzer (charge purifier) to remove from the beam any ions that gained or lost electrons in collisions with background gas atoms. Immediately after this analyzer, the ion beam was crossed at right angles by a magnetically confined electron beam. Typical electron currents were 300 μA at 100 V accelerating voltage and 2.5 mA at 500 V. Immediately after the collision region, the ions entered a parallel-plate electrostatic analyzer which separated parent ions of charge q from product ions of charge $q+1$. The parent-ion-beam

 ©1986 The American Physical Society

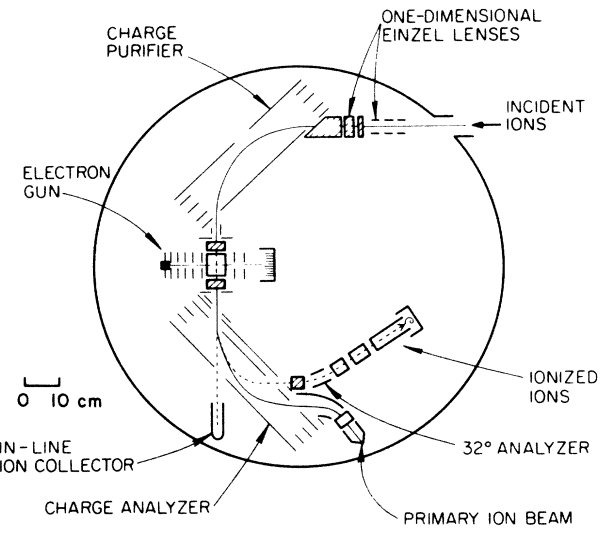

FIG. 1. A schematic diagram of the crossed-beam apparatus used to measure electron-impact ionization cross sections for the multiply charged ions S^{4+}, Cl^{5+}, and Ar^{6+}.

current was measured by collecting it in a Faraday cup biased to suppress the loss of secondary electrons, and the product ions were counted by a channel electron multiplier operated in a pulse-counting mode. At 200 eV electron energy, typical product signal and background count rates were 25 and 60 s^{-1} for S^{4+}, 60 and 350 s^{-1} for Cl^{5+}, and 200 and 1500 s^{-1} for Ar^{6+}. The electron-beam current was measured by collecting it in a suppressed collector designed to minimize the number of electrons reflected back along the magnetic-field lines into the collision region.

From the measured quantities, the cross section at energy E is determined from the equation

$$\sigma(E)=\frac{R}{I_i I_e}\frac{qe^2 v_i v_e}{(v_i^2+v_e^2)^{1/2}}\frac{F}{D}, \tag{3}$$

where R is the product-ion count rate, qe is the charge of the incident ions, e is the charge on an electron, I_i and I_e are the incident ion and electron currents, v_i and v_e are the ion and electron velocities, F is a geometrical factor taking into account the spatial overlap of the two beams, and D is the detection efficiency for the product ions.

The exit slits in the post-collision analyzer were designed with an enlarged slit for the parent beam, so that when a 5+, 6+, or 7+ product beam was deflected to the detector, the corresponding 4+, 5+, or 6+ parent beam was collected in the Faraday cup. The arrangement allowed the same analyzer to be used for all three incident multiply charged ions. The electron beam was chopped so that detector counts due to electron-impact ionization could be separated from background counts. Part of this background was due to stripping on background gas between the two parallel-plate analyzers, and part resulted from photons produced when energetic ions hit surfaces in the chamber. Since the ions can be focused or deflected by the space charge of the electron beam,[18] the background may be modulated by the chopped electron beam, mimicking the behavior of the true ionization signal. Such a spurious space-charge modulation signal was observed for incident Cl^{5+} and Ar^{6+} (but not for S^{4+}) below the energy threshold for electron-impact ionization. To correct for this, a curve with the functional dependence $1/v_e$, where v_e is the electron velocity, was fitted to the below-threshold data and was subtracted from the apparent cross section above threshold. The functional form of this correction is that expected[18,19] if the degree of background modulation is proportional to the charge density in the electron beam. This correction due to the spurious space-charge modulation signal was 5% at the peak of the cross section for Cl^{5+} and 3% at the peak of the cross section for Ar^{6+}.

Figure 2(a) shows the uncorrected apparent cross section for Cl^{5+} in the threshold region. The solid line is the $1/v_e$ fit to the below-threshold measurements. Figure 2(b) shows the corrected cross section. The most significant uncertainty introduced by this correction is in the location of the experimental ionization onset, and hence in the estimates one may make of the fraction of metastable $3s\,3p\,^3P$ ions in the incident beam.

Uncertainties in the measured quantities of Eq. (3) are listed in Table I. The uncertainties are listed at good-confidence level, equivalent to a 90%-confidence level for the statistical uncertainty in the product-ion count rate R.

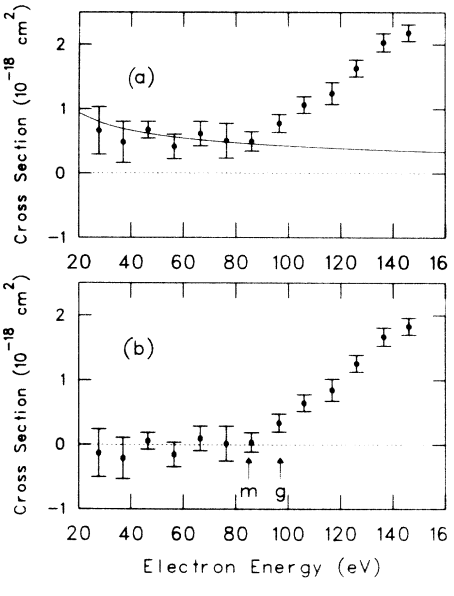

FIG. 2. (a) The apparent cross section for ionization of Cl^{5+} as a function of electron energy, including a spurious contribution from space-charge modulation of background counts. Solid line is a fit of the form $\sigma=A/v_e$ to the points below 80 eV. (b) The corrected cross section determined by subtracting the solid line of Fig. 2(a) from the apparent cross section. Arrows labeled g and m mark the ionization thresholds from ground-level $2p^6 3s^2$ and metastable $2p^5 3s\,3p$ Cl^{5+} ions, respectively.

TABLE I. Cross-section uncertainties. All uncertainties are listed at the good-confidence level [equivalent to 90%-confidence level (90% CL) or two standard deviations on statistical uncertainties].

Source	Uncertainty (%) S^{4+}	Cl^{5+}	Ar^{6+}
Statistical uncertainty (typical value at peak cross section at 90% CL)	±4	±6	±3
Form factor	±4	±4	±4
Systematic uncertainties:			
Particle counting efficiency	±3	±3	±3
Transmission to signal ion detector	±4	±4	±4
Ion current	±4	±2	±2
Electron current	±2	±2	±2
Ion and electron velocities	±1	±1	±1
Background modulation correction		±2	±2
Quadrature sum: total uncertainty (good confidence) at the peak of the cross section	±9	±10	±8

III. RESULTS

A. S^{4+}

The measured cross sections for electron-impact ionization of S^{4+} are tabulated in Table II and shown in Fig. 3. The error bars indicated on Fig. 3 are relative uncertainties due to counting statistics, at the one standard-deviation level. Additional systematic uncertainties which apply to S^{4+}, Cl^{5+}, and Ar^{6+} are listed in Table I.

The most striking feature in the cross-section curve is the abrupt change in slope that occurs near 170 eV. This is due to the onset of the indirect excitation-autoionization process which we attribute to $2p$-nl excitation [Eq. (2)]. We estimate the peak cross section for EA for this case to be 2.5×10^{-18} cm^2. The indirect process appears to contribute an important fraction to the total ionization cross section for this ion. We estimate the ratio of the peak indirect to peak direct cross sections for S^{4+} to be about 0.5.

The threshold energy for removal of one electron from the ground ^1S level of S^{4+} is 72.7 eV. Our observed threshold is lower, near the 62.5 eV threshold for ionization from the metastable $3s\,3p\,^3P$ levels, which indicates that there is a substantial metastable population in the

TABLE II. Electron-impact ionization cross sections for S^{4+}. Uncertainties are one standard deviation on counting statistics. See Table I for total uncertainties.

E (eV)	σ (10^{-18} cm^2)	E (eV)	σ (10^{-18} cm^2)	E (eV)	σ (10^{-18} cm^2)
37.3	0.12±0.17	142	4.35±0.10	256	7.30±0.09
47.2	0.25±0.14	147	4.93±0.12	265	7.10±0.09
57.1	0.20±0.11	152	4.75±0.10	275	6.89±0.07
61.2	0.18±0.14	157	4.66±0.13	285	6.93±0.09
64.2	0.28±0.15	162	4.83±0.13	292	6.94±0.07
67.0	0.56±0.16	167	4.95±0.13	317	6.74±0.09
69.9	0.80±0.15	171	5.31±0.13	341	6.57±0.09
72.0	1.14±0.18	177	5.44±0.13	367	6.44±0.09
74.0	1.23±0.12	181	5.92±0.13	391	6.31±0.09
76.8	1.37±0.11	186	6.17±0.14	440	6.26±0.09
79.0	1.84±0.16	191	6.27±0.08	490	6.29±0.07
81.9	2.19±0.17	194	6.24±0.07	539	6.16±0.18
83.1	2.03±0.15	198	6.74±0.07	589	5.76±0.09
86.9	2.46±0.11	200	6.57±0.14	638	5.72±0.09
91.7	2.92±0.15	203	6.62±0.14	689	5.56±0.06
102.4	3.59±0.13	206	6.75±0.14	839	4.97±0.07
112.3	3.75±0.13	209	6.73±0.14	992	4.40±0.07
122.9	4.48±0.13	216	6.98±0.09	1195	3.97±0.07
127	4.33±0.13	236	7.21±0.09	1392	3.68±0.07
137	4.47±0.13				

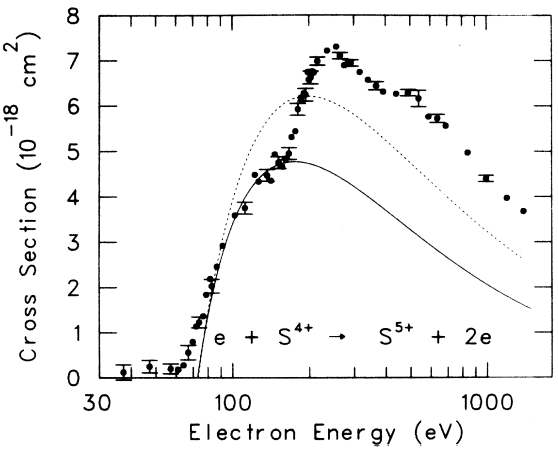

FIG. 3. Cross sections for electron-impact ionization of S^{4+}. Experiment: ●, present results. Theory: — — —, Lotz semiempirical formula, Ref. 3; ——, distorted-wave result for Ar^{6+} (Ref. 21) scaled to S^{4+} by Eq. (4). The change in slope near 160 eV is attributed to the onset of $2p$-nl excitation-autoionization.

S^{4+} beam produced by the ECR source. On the basis of statistical weights alone, we would expect a significant fraction of the S^{4+} ions to be in metastable ^3P levels; such a statistical distribution is consistent with earlier observations for Be-like ions.[20]

Measurements of the electron-impact ionization cross section for S^{4+} were made using the two isotopes ^{32}S and ^{34}S, which were present in the source in their naturally occurring abundances (95% ^{32}S and 4.2% ^{34}S). The two isotopes were well resolved by the 90° ion-source bending magnet. Measurements using $^{34}S^{4+}$ were independently absolute but were time consuming because of the small current of $^{34}S^{4+}$ ions available. Measurements using $^{32}S^{4+}$ could be made much more quickly, since the ion current was larger than for $^{34}S^{4+}$ by a factor of 20, but were not independently absolute since the $^{32}S^{4+}$ beam was contaminated with a small amount of $^{16}O^{2+}$, which has the same mass-per-charge ratio. The O^{3+} signal due to ionization of the O^{2+} contaminant was rejected by the post-collision charge analyzer, so the only effect of the contaminant was that the measured incident ion current [I_i in Eq. (3)] was larger than the actual $^{32}S^{4+}$ incident current.

The shape of the ionization cross section versus electron energy for S^{4+} was measured using $^{32}S^{4+}$ and normalized to the absolute magnitude measured at a few electron energies using $^{34}S^{4+}$. The normalization of the $^{32}S^{4+}$ data amounted to a 7% change, implying that 14% of the particles in the beam were O^{2+} ions. The total uncertainty at the peak of the cross section is estimated to be ±9% at good-confidence level, including both random and systematic errors.

The solid curve in Fig. 3 is the DWE result of Younger[21] for Ar^{6+} scaled to S^{4+} by the prescription

$$\sigma(E)=\frac{(124.3)^2}{E_I^2}f(E/E_I)\ , \tag{4}$$

where E is the energy of the incident electron in eV, E_I is the ionization potential of the ion in eV, and $f(E/E_I)$ is the cross section given by Younger for ground-state Ar^{6+} as a function of the electron energy in ionization threshold units. It is expected that the actual scaling of the direct-ionization cross section along an isoelectronic sequence is not exactly as given here,[22] but for the ions considered in this paper, this scaled result is in excellent agreement with the experimental data (below the threshold for indirect ionization) except in the threshold region when metastables in the incident beam have shifted the experimental onset to lower energy. Calculations using the Lotz[3] formula lead to an overestimation of the cross section for direct ionization of S^{4+} by about 30%.

For S^{4+} there is an apparent additional structure ($\approx 0.5\times10^{-18}$ cm^2) in the cross section with an onset near 400 eV and a peak near 550 eV. The feature has the shape one may expect of a cross section for excitation, and excitation of $2s$ electrons comes to mind until it is realized that $2s$ electrons ionize at 304 eV—well below the onset of the feature. Thus we have no explanation for this feature.

B. Cl^{5+}

The cross sections for ionization of Cl^{5+} are tabulated in Table III and shown in Fig. 4. The error bars in Fig. 4 represent random uncertainties at one standard deviation. The systematic uncertainties are listed in Table I. These include a systematic uncertainty due to the correction for space-charge modulation described in Sec. II. We estimate the magnitude of this uncertainty to be 0.2×10^{-18} cm^2 at threshold, decreasing to 0.1×10^{-18} cm^2 at the peak of the cross section.

As is the case with S^{4+}, a change in the slope of the

TABLE III. Electron-impact ionization cross sections for Cl^{5+}. Uncertainties are one standard deviation on counting statistics. See Table I for total uncertainties.

E (eV)	σ (10^{-18} cm^2)	E (eV)	σ (10^{-18} cm^2)
66.5	0.10±0.19	235	3.96±0.08
76.4	0.02±0.27	250	4.43±0.07
86.9	0.04±0.15	255	4.55±0.08
96.5	0.34±0.14	275	4.70±0.09
107.4	0.65±0.13	294	4.95±0.05
116.7	0.85±0.17	306	4.83±0.05
126.9	1.26±0.13	319	4.62±0.05
136.4	1.67±0.14	344	4.72±0.05
147.2	1.83±0.13	368	4.47±0.15
156.1	1.92±0.13	393	4.60±0.05
176	2.34±0.11	441	4.59±0.09
186	2.37±0.11	491	4.50±0.05
195	2.48±0.08	540	4.46±0.09
202	2.93±0.10	591	4.25±0.05
210	2.99±0.09	690	4.03±0.05
211	3.30±0.09	840	3.71±0.05
214	3.82±0.09	992	3.54±0.05
215	3.72±0.07	1193	3.25±0.05
220	3.51±0.09	1393	3.05±0.05
225	3.82±0.07		

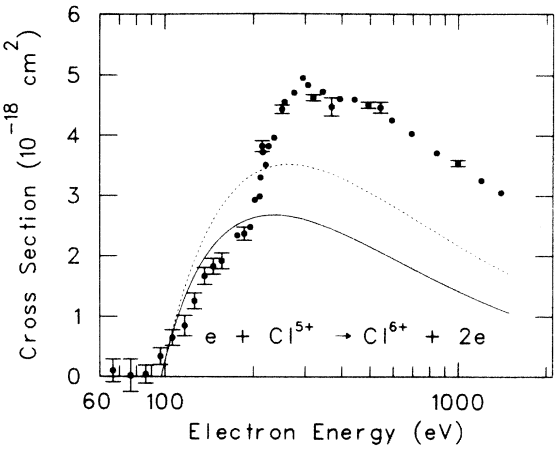

FIG. 4. Cross sections for electron-impact ionization of Cl^{5+}. Experiment: ●, present results. Theory: — — —, Lotz semiempirical formula, Ref. 3; ——, distorted-wave result for Ar^{6+} (Ref. 21) scaled to Cl^{5+} by Eq. (4). The change in slope near 200 eV is attributed to the onset of $2p$-nl excitation-autoionization.

cross section as a function of energy (near 200 eV for Cl^{5+}) marks the onset of indirect ionization due to $2p$-nl excitation to autoionizing levels. We estimate the peak of the indirect contribution to be 2.5×10^{-18} cm^2 and of the direct contribution to be 2.5×10^{-18} cm^2, thus giving a ratio of the indirect to direct peak cross sections of 1.0.

The observed ionization threshold is near 85 eV, again indicating a significant fraction of metastable $3s\,3p\,^3P$ ions in the incident beam, since the ionization threshold for the $3s^2\,^1S$ ground-state level is 97 eV.

For Cl^{5+}, as for S^{4+}, the cross sections for direct ionization obtained from the Lotz[3] semiempirical formula (dashed line in Fig. 4) are about 30% larger than measured. The solid curve in Fig. 4 is the DWE result[21] for direct ionization of Ar^{6+}, scaled to Cl^{5+} using Eq. (4); and agreement with the measurements is good below the threshold for indirect ionization. As was the case for S^{4+}, there may be an additional feature in the Cl^{5+} cross section in the 400—500-eV region, but less pronounced in this case. Again, we are aware of no mechanism which might produce such a feature, and have no explanation.

C. Ar^{6+}

The cross sections for electron-impact ionization of Ar^{6+} are given in Table IV and Fig. 5. The error bars are random uncertainties at one standard deviation. The systematic uncertainties are listed in Table I. As for Cl^{5+}, there is a systematic uncertainty due to the correction for space-charge modulation of the ion beam. We estimate this uncertainty at good-confidence level to be $\pm0.10\times10^{-18}$ cm^2 at threshold and $\pm0.05\times10^{-18}$ cm^2 at the peak of the cross section.

The dashed curve in Fig. 5 is the prediction of the Lotz[3] semiempirical formula for the direct-ionization cross section [process (1)] and is about 17% larger than measured. The solid line represents the DWE calculation of Younger[21] and the values are about 15% smaller than measured. The peak magnitudes of the direct and indirect contributions to the total ionization cross section are each about 2×10^{-18} cm^2 with, however, the EA contribution being slightly larger to give a ratio of about 1.1.

TABLE IV. Electron-impact ionization cross sections for Ar^{6+}. Uncertainties are typical relative uncertainties, which combine one standard deviation on counting statistics with uncertainties in the form factor. See Table I for total uncertainties.

E (eV)	σ (10^{-18} cm^2)	E (eV)	σ (10^{-18} cm^2)
36.5	0.00	270	2.81
56.5	−0.02±0.05	275	2.98
76.5	0.01	295	3.24
96.5	0.04	320	3.47±0.07
107	0.08	345	3.58
117	0.08±0.05	370	3.70
126	0.32	395	3.68
137	0.66	445	3.62
147	0.92	495	3.57±0.05
156	1.05	543	3.47
166	1.19±0.07	593	3.38
176	1.34	642	3.27
186	1.48	693	3.20
196	1.51	793	2.96±0.05
216	1.67	893	2.80
236	1.86±0.07	996	2.69
241	1.94	1100	2.58
246	2.09	1202	2.52
251	2.14	1298	2.45±0.05
255	2.30	1398	2.41
260	2.53	1503	2.34
265	2.77		

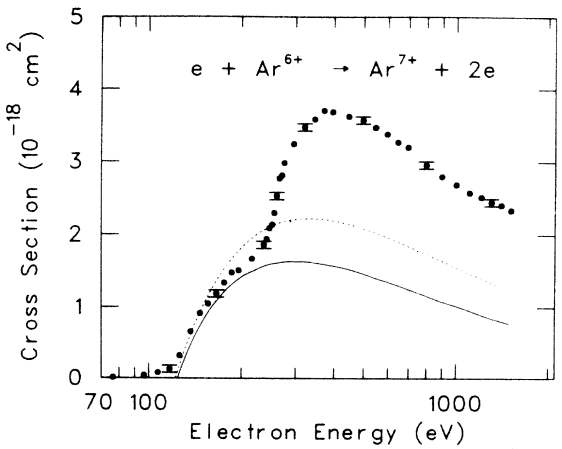

FIG. 5. Cross sections for electron-impact ionization of Ar^{6+}. Experiment: ●, present results. Theory: — — —, Lotz semiempirical formula, Ref. 3; ——, distorted wave with exchange, Ref. 21. The change in slope near 240 eV is attributed to the onset of $2p$-nl excitation-autoionization.

IV. DISCUSSION

The present measurements show the increasing relative importance of $2p$-nl excitation-autoionization with increasing ionic charge along the Mg-isoelectronic sequence. Estimates of the EA contributions may be obtained using the well-known Gaunt factor formula for ion excitation:[23]

$$\sigma_{\bar{g}}(X)=\frac{8\pi}{\sqrt{3}}\frac{R^2}{\Delta^2}\frac{\bar{g}(X)}{X}f\pi a_0^2 . \quad (5)$$

Here, R is the Rydberg energy (13.6 eV), Δ is the excitation threshold energy, $\bar{g}(X)$ is the effective Gaunt factor at energy X, X is the energy in threshold units ($X=E/\Delta$), and f is the oscillator strength for the transition.

Indicated in Table V are the experimental ratios ρ of the peak indirect-ionization to peak direct-ionization cross sections including measurements of Belić *et al.*[24] for Al^+. As already noted, the ratio ρ shown in the table is seen to increase monotonically with atomic number over this range of Z. The excitation cross sections decrease only slowly with Z, whereas the direct-ionization cross section decreases roughly as $1/Z^2$. Of course, for higher Z radiative stabilization of the core-excited states will become relatively more important.

Figure 6 shows the result when the cross sections from scaled distorted-wave estimates for direct ionization (slightly normalized to the data points just below threshold for EA) are subtracted from the measured total cross sections for ionization of Cl^{5+}. This difference should represent the cross sections for EA provided no other

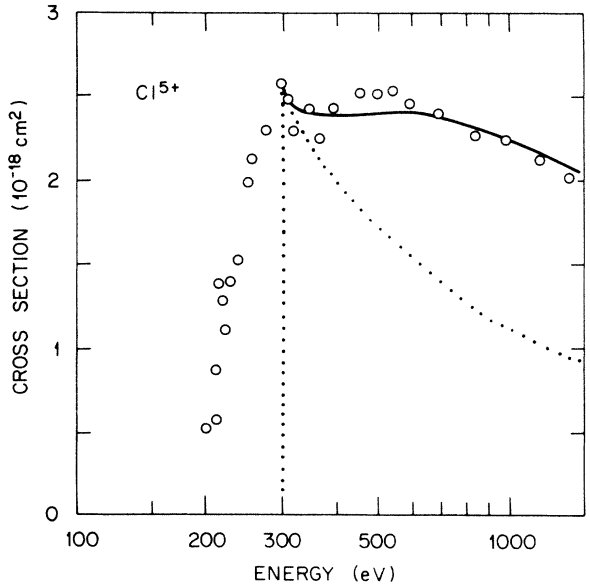

FIG. 6. Estimate of the experimental cross sections for indirect electron-impact ionization of Cl^{5+} determined by subtracting scaled distorted-wave estimates for direct-ionization cross sections from the measured total ionization cross sections. Dotted curve represents the $\bar{g}$ formula [Eq. (5)] scaled to the experimental data for $\Delta=300$ eV (see text). Solid curve is the sum of the dotted curve and the SPWB cross section curve for direct $2p$ ionization of Cl^{5+} from Ref. 13.

TABLE V. Comparison of measured peak EA and direct contributions to ionization of Mg-like ions. Al^+ measurements are from Belić *et al.* (Ref. 24).

Ion	σ_{EA}^m (10^{-18} cm^2)	σ_{dir}^m (10^{-18} cm^2)	$\rho=\sigma_{EA}^m/\sigma_{dir}^m$
Al^+	4	72	0.06
S^{4+}	2.5	4.8	0.5
Cl^{5+}	2.5	2.5	1.0
Ar^{6+}	2	1.8	1.1

mechanisms contribute to ionization. It is instructive to compare the energy dependence shown in this figure to that expected for an excitation cross section. The dotted curve in Fig. 6 represents Eq. (5) plotted for an f value adjusted to give the measured peak cross section for Δ taken just below the 303-eV threshold for ionization of $2p$ electrons. This curve indicates the expected falloff of the $2p$-nl EA contributions at energies above the highest EA threshold, and does not reproduce the individual EA onsets which occur in the 200—300-eV range. It is seen that the measured data fall off much more slowly than this model curve for excitation of dipole-allowed levels, indicating the possible contribution of another mechanism to the observations. The solid curve in Fig. 6 results when the cross sections for ionization of the $2p$ electrons calculated by McGuire[13] using the SPWB method are added to the dotted curve. The agreement of the solid curve with the data points in the figure is very good, giving strong evidence that ionization of the $2p$ electrons contributes with a large branching ratio to single ionization of Cl^{5+}. Similar analyses have been applied to the S^{4+} and Ar^{6+} data, and result in the same conclusion.

Figure 7 shows a number of calculated energy levels[14] for the ions S^{4+}, S^{5+}, and S^{6+}. It may be seen for S^{4+}—and indeed it is true for all the ions in this study—that the

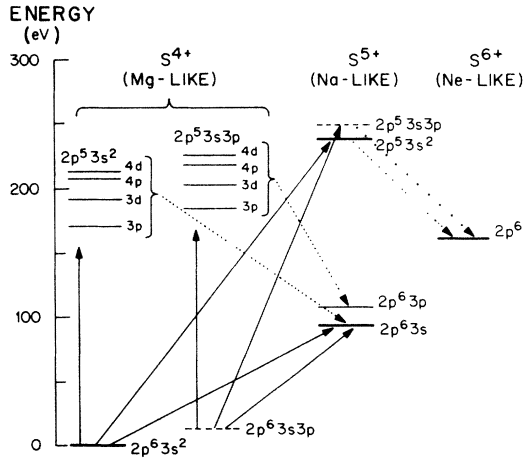

FIG. 7. Calculated energy levels (from Ref. 14) and important transitions in the electron-impact ionization of Mg-like S^{4+}. Vertical arrows denote excitation processes, inclined arrows denote direct ionization, and dotted arrows denote autoionization pathways. Dashed energy levels indicate metastability against radiative or Auger decay.

energy to remove a $2p$ electron is much more than that needed to lead to the ultimate ejection of two electrons. It thus is expected that the decay mode of the $2p^5 3s^2$ core-excited state will be predominantly by autoionization,[25] which will result in a net double ionization and thus not contribute to the present single-ionization measurements. It was noted, however, in Sec. III that the experimentally observed ionization onsets suggest that a significant fraction of the incident Mg-like ions produced in the ECR source are in the $2p^6 3s 3p\ ^3P$ metastable levels. Ejection of a $2p$ electron from such a metastable configuration can produce doublet and quartet levels of the Na-like $2p^5 3s\ 3p$ configuration which are metastable against autoionization.[26] Indeed the Na-like ions extracted directly from the ECR source (e.g., S^{5+}, Cl^{6+}, Ar^{7+}) produced large autoionizing backgrounds which precluded accurate ionization cross-section measurements for these ions. The measured ionization background normalized to incident ion intensity is shown in Fig. 8 for a number of Na-like ions. By varying the velocity of the S^{5+} beam, we were able to deduce that the mean lifetimes of these levels against autoionization were in the 10-μs range for this ion.

In the present experiment $2p^5 3s\ 3p$ Na-like ions are produced by $2p$ ionization of $2p^6 3s\ 3p$ metastable Mg-like ions in the crossed-beam collision region. The lifetimes of the metastable levels are sufficiently long that only a fraction of these product ions will autoionize before the post-collision charge analysis and detection. Thus $2p$ inner-shell ionization of metastable Mg-like ions will contribute primarily to the observed single-ionization cross section, thereby substantiating our earlier conclusions based on the analysis presented in Fig. 6. More detailed calculations using the distorted-wave approximation may be found in the accompanying paper by Pindzola *et al.*[14]

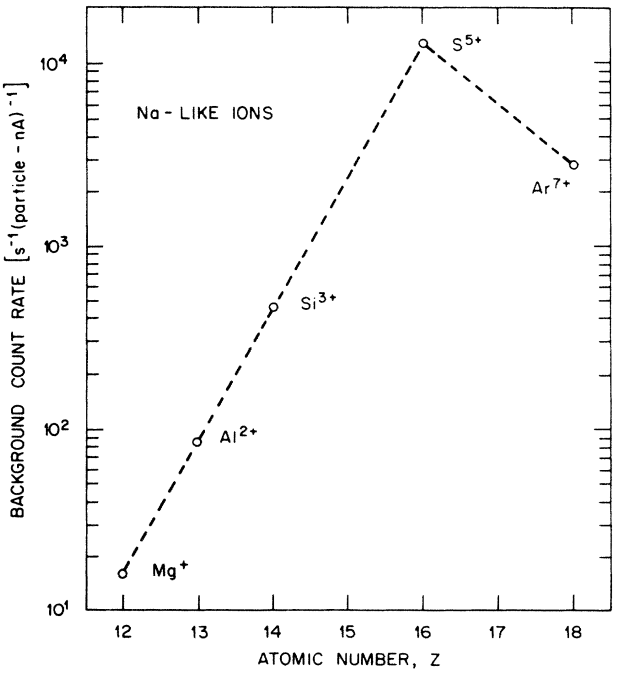

FIG. 8. Measured background count rate in the ionization channel, normalized to the incident ion flux of several Na-like ions. This background is independent of residual gas pressure and is attributed to the presence in the beam of $2p^5 3s\ 3p$ metastable ions having lifetimes against autoionization in the 1—10-μs range.

The present results for Cl^{5+} (Fig. 4) show a strong initial rise near 210 eV and another emphatic rise near 250 eV. We associate the first rise with the monopole $2p$-$3p$ excitation, and the second with the $2p$-$3d$ excitation. The rise for Ar^{6+} (Fig. 5) at about 250 eV is associated with the $2p$-$3p$ transition. In S^{4+} (Fig. 3) the rise near 170 eV is associated with $2p$-$3p$ excitation, and that near 200 eV with the $2p$-$3p$ transition. Thus we conclude that for the Mg-like ions, the $2p$-$3p$ transitions are relatively strong and contribute substantially to EA. One of the striking features in the experimental data[27] on Na-like ions was the fact that the monopole $2p$-$3p$ excitation cross section seemed to be much smaller than predicted.[11] These excitations produce the same $2p^5 3s\ 3p$ configurations, some levels of which, as noted above, are metastable against autoionization. In our experiments on Na-like ions, this metastability prevents single ionization before detection, whereas for Mg-like ions, it prevents double ionization before detection.

V. SUMMARY

We have measured cross sections for electron-impact ionization of three members of the Mg-isoelectronic sequence. The cross section for direct-ionization scales approximately as E_I^{-2}, where E_I is the ionization potential. There are substantial excitation-autoionization contributions due to $2p$-nl transitions and the relative importance of this EA mechanism increases with Z along this portion of the isoelectronic sequence. Major fractions of Mg-like ions extracted from the ECR source are in metastable $2p^6 3s\ 3p$ levels. Inner-shell ionization of $2p$ electrons from these metastable ions contribute to single ionization in our experiment, due to the metastability against autoionization of levels in the resulting $2p^5 3s\ 3p$ configuration. This evidence may help us to resolve some outstanding issues raised by earlier experiments on Na-like ions.

ACKNOWLEDGMENTS

The authors are grateful to C. Bottcher, M. S. Pindzola, and D. C. Griffin for many fruitful discussions, and for providing their energy-level calculations to us. Special thanks are also due to R. J. W. Henry and E. J. McGuire for communicating information about unpublished research in progress. This work was sponsored by the Office of Fusion Energy of the U.S. Department of Energy under Contract No. DE-AC05-840R21400 with Martin Marietta Energy Systems, Inc., and Contract No. DE-AI01-76PR06010 with the National Bureau of Standards. A.M.H. acknowledges support from the U.S. Department of Energy, through Oak Ridge Associated Universities, and A. Müller from the JILA Visiting Fellow Program and from the Max Kade Foundation.

*Present address: GA Technologies, San Diego, CA 92138.
†Permanent address: Institut für Kernphysik, Universität Giessen, West Germany.
‡Permanent address: Institute of Physics, Belgrade, Yugoslavia.

[1]R. A. Hulse, Nucl. Technol. **3**, 259 (1983).
[2]D. L. Matthews *et al.*, Phys. Rev. Lett. **54**, 110 (1985).
[3]W. Lotz, Z. Phys. **216**, 241 (1968).
[4]E. J. McGuire, Phys. Rev. A **3**, 267 (1971); **16**, 62 (1977); **20**, 445 (1979).
[5]R. E. H. Clark and D. H. Sampson, J. Phys. B **17**, 3311 (1984); L. B. Golden and D. H. Sampson, *ibid.* **13**, 2645 (1980); D. L. Moores, L. B. Golden, and D. H. Sampson, *ibid.* **13**, 385 (1980); L. B. Golden, D. H. Sampson, and K. Omidvar *ibid.* **11**, 3235 (1978); D. H. Sampson and L. B. Golden, *ibid.* **11**, 541 (1978).
[6]S. M. Younger, Phys. Rev. A **24**, 1278 (1981); **24**, 1272 (1981); **23**, 1138 (1981); **22**, 1425 (1980).
[7]A. Burgess and M. C. Chidichimo, Mon. Not. R. Astron. Soc. **203**, 1269 (1983).
[8]D. H. Sampson and L. B. Golden, J. Phys. B **14**, 903 (1981); **12**, L785 (1979).
[9]D. H. Sampson, J. Phys. B **15**, 2087 (1982).
[10]D. C. Griffin, M. S. Pindzola, and C. Bottcher, J. Phys. B **17**, 3183 (1984); M. S. Pindzola, D. C. Griffin, and C. Bottcher, Phys. Rev. A **27**, 2331 (1983).
[11]D. C. Griffin, C. Bottcher, and M. S. Pindzola, Phys. Rev. A **25**, 154 (1982).
[12]R. J. W. Henry and A. Z. Msezane, Phys. Rev. A **26**, 2545 (1982).
[13]E. J. McGuire (private communication).
[14]M. S. Pindzola, D. C. Griffin, and C. Bottcher, following paper, Phys. Rev. A **33**, 3787 (1986); private communication.
[15]S. S. Tayal and R. J. W. Henry (private communication).
[16]D. H. Crandall, R. A. Phaneuf, and P. O. Taylor, Phys. Rev. A **18**, 1911 (1978).
[17]F. W. Meyer, Nucl. Instrum. Methods B **9**, 532 (1985).
[18]M. F. A. Harrison, Br. J. Appl. Phys. **17**, 371 (1966).
[19]K. T. Dolder, in *Case Studies in Atomic Collision Physics I*, edited by E. W. McDaniel and M. R. C. McDowell (North-Holland, Amsterdam, 1969), pp. 257–260.
[20]R. A. Falk, G. Stefani, R. Camilloni, G. H. Dunn, R. A. Phaneuf, D. C. Gregory, and D. H. Crandall, Phys. Rev. A **28**, 91 (1983).
[21]S. M. Younger, *Atomic Data for Fusion*, Vol. 7, p. 190 (1981), Controlled Fusion Atomic Data Center Newsletter, Oak Ridge National Laboratory (unpublished).
[22]S. M. Younger, Phys. Rev. A **22**, 111 (1980).
[23]H. Van Regemorter, Astrophys. J. **136**, 906 (1962).
[24]D. S. Belić, R. A. Falk, C. Timmer, and G. H. Dunn (private communication).
[25]M. H. Chen and B. Crasemann, Phys. Rev. A **10**, 2232 (1974).
[26]S. E. Harris, D. J. Walker, R. G. Caro, A. J. Mendelsohn, and R. D. Cowan, Opt. Lett. **9**, 168 (1984).
[27]D. H. Crandall, R. A. Phaneuf, R. A. Falk, D. S. Belić, and G. H. Dunn, Phys. Rev. A **25**, 143 (1982).